ACADEMIC PRESS

Available online at www.sciencedirect.com

SCIENCE DIRECT®

Journal of Magnetic Resonance 161 (2003) 265–274

JMR Journal of Magnetic Resonance

www.elsevier.com/locate/jmr

Communication

Resolution enhancement in in vivo NMR spectroscopy: detection of intermolecular zero-quantum coherences

Cornelius Faber,* Eberhard Pracht, and Axel Haase

Physikalisches Institut, Universität Würzburg, Am Hubland, Würzburg D-97074, Germany

Received 2 October 2002; revised 23 December 2002

Abstract

Intermolecular zero-quantum coherences are insensitive to magnetic field inhomogeneities. For this reason we have applied the HOMOGENIZED sequence [Vathyam et al., Science 272 (1996) 92] to phantoms containing metabolites at low concentrations, phantoms with air inclusions, an intact grape, and the head of a rat in vivo at 750 MHz. In the ^{1}H-spectra, the water signal is efficiently suppressed and line broadening due to susceptibility gradients is effectively removed along the indirectly detected dimension. We have obtained a ^{1}H-spectrum of a 2.5 mM solution of γ-aminobutyric acid in 12 min scan time. In the phantom with air inclusions a reduction of line widths from 0.48 ppm in the direct dimension to 0.07 ppm in the indirect dimension was observed, while in a deshimmed grape the reduction was from 1.4 to 0.07 ppm. In a spectrum of the grape we were able to resolve glucose resonances at 0.3 ppm from the water in 6 min scan time. *J*-coupling information was partly retained. In the in vivo spectra of the rat brain five major metabolites were observed.

Keywords: In vivo NMR spectroscopy; iZQC; HOMOGENIZED; Dipolar demagnetizing field; Resolution enhancement

1. Introduction

The latest generation of wide bore magnets, with a field strength of 17.6 T, promises enhanced resolution and improved signal to noise ratio (SNR) for in vivo applications of NMR spectroscopy. The SNR dependence on B_0 is between linear and $B_0^{7/4}$ in a typical in vivo experiment. However, inhomogeneous line broadening due to magnetic susceptibility gradients caused by interfaces between tissue and air, bone, capillary vessels, or just different tissue types leads in vivo to severe problems with water suppression and signal overlap. While several methods have been developed to efficiently suppress unwanted signal from tissue water in regions with homogeneous B_0 [1], the problem of line broadening itself remains unsolved. The most fundamental tool against inhomogeneous line broadening, shimming, can only alleviate this problem if inhomogeneities are caused by macroscopic susceptibility gradients. Tissue with microscopic air inclusions, such as the lungs of mammals or leaves of plants, are generally acknowledged to be inaccessible for NMR spectroscopy at high frequencies. Only a few methods are known to be able to fundamentally tackle this problem. The spin echo sequence refocuses inhomogeneous line broadening, but it also eliminates chemical shift differences and perturbs *J*-coupling, the two most important pieces of information from NMR spectroscopy. In the case of well defined gradients of the static magnetic field, it has been shown that line broadening can be refocused by nutation echoes induced with matched radiofrequency gradients [2]. However, for tissue with complex field gradients it seems unlikely that matched radiofrequency fields can be created. Another method, termed total spin coherence transfer echo spectroscopy [3], has been proposed that is insensitive to field inhomogeneities. However, uncoupled spins do not contribute to the observed signal and thus the method is in general not suitable for in vivo applications. Warren and co-workers [4] have proposed a sequence termed HOMOGENIZED (homogeneity enhancement by intermolecular zero-quantum detection) that exploits intermolecular zero-quantum coherences (iZQC) and yields two-dimensional (2D) spectra

* Corresponding author. Fax: +49-931-888-5851.
E-mail address: faber@physik.uni-wuerzburg.de (C. Faber).

1090-7807/03/$ - see front matter © 2003 Elsevier Science (USA). All rights reserved.
doi:10.1016/S1090-7807(03)00006-5

that are insensitive to field inhomogeneities along the indirectly detected dimension. Results using this method have been shown for a deshimmed sample in a high resolution probe [4] and in a strongly drifting magnet [5]. It was also suggested that this method could be applied in vivo [4].

Here we report the first application of the HOMOGENIZED sequence for in vivo spectroscopy at 17.6 T. Inhomogeneous line broadening in the ^{1}H-spectra due to microscopic susceptibility differences is substantially removed and the water signal is efficiently suppressed.

2. Properties of HOMOGENIZED spectra

The HOMOGENIZED sequence as suggested by Vathyam et al. [4] is shown in Fig. 1. It exploits long range dipolar field effects that can be theoretically explained in the classical picture with the dipolar demagnetizing field [6–8] or with quantum mechanics via multiple-quantum coherences [9–11]. We now discuss the features of the HOMOGENIZED sequence in a typical in vivo application.

Coherences contributing to the detected signal for a system of a spin I (metabolite) and an inequivalent spin S (water) are indicated in Fig. 1. The first 90°-pulse excites all single- and multiple-quantum coherences [9]. These develop in the 2D experiment during the incremented time t_1. Only zero-quantum coherences ultimately contribute to the detected signal since the applied gradient pulse dephases all other coherences. The 45°-pulse converts the zero-quantum coherences into I_zS_y and S_zI_y coherences which are converted into observable magnetization by dipolar couplings during the interval 2Δ and the acquisition time t_2. A 2D Fourier transformation with respect to t_1 and t_2 yields a 2D spectrum with four cross peaks appearing at their Larmor frequencies ω_I and ω_S along f_2 and at the frequency differences $\omega_I - \omega_S$ and $\omega_S - \omega_I$ along f_1, corresponding to p-type and n-type coherences. Ahn et al. [12] have shown that, neglecting relaxation effects and radiation damping, the magnetization for the cross peak at $(\omega_I - \omega_S, \omega_I)$ develops as:

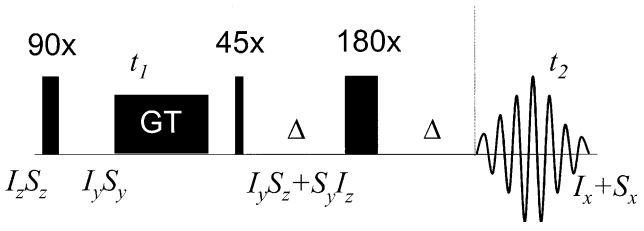

Fig. 1. Pulse sequence of the HOMOGENIZED experiment [4]. Relevant product operators for a system of two inequivalent spins (water, metabolite) are indicated.

$$M^{\mathrm{I,Obs}} \propto M_0^{\mathrm{I}} \times \left\{ \cos\frac{\pi}{4} \times J_0\left(-\sin\frac{\pi}{4} \times \frac{t_2}{\tau_{\mathrm{D,I}}} \right) - \frac{1-\cos(\pi/4)}{\sin(\pi/4)} \frac{\tau_{\mathrm{D,I}}}{t_2} \times J_1\left(-\sin\frac{\pi}{4} \times \frac{t_2}{\tau_{\mathrm{D,I}}} \right) \right\} \times J_1\left(-\sin\frac{\pi}{4} \times \frac{2}{3}\frac{t_2}{\tau_{\mathrm{D,S}}} \right), \quad (1)$$

and for the cross peak at $(\omega_S - \omega_I, \omega_I)$ as:

$$M^{\mathrm{I,Obs}} \propto M_0^{\mathrm{I}} \times \left\{ \cos\frac{\pi}{4} \times J_2\left(-\sin\frac{\pi}{4} \times \frac{t_2}{\tau_{\mathrm{D,I}}} \right) - \frac{1-\cos(\pi/4)}{\sin(\pi/4)} \frac{\tau_{\mathrm{D,I}}}{t_2} \times J_1\left(-\sin\frac{\pi}{4} \times \frac{t_2}{\tau_{\mathrm{D,I}}} \right) \right\} \times J_1\left(-\sin\frac{\pi}{4} \times \frac{2}{3}\frac{t_2}{\tau_{\mathrm{D,S}}} \right), \quad (2)$$

where J_n is the nth order Bessel function and $\tau_{\mathrm{D,I/S}} = (\gamma\mu_0 M_0^{\mathrm{I/S}})^{-1}$ the demagnetizing time, where γ is the gyromagnetic ratio, μ_0 the vacuum permeability, and $M_0^{\mathrm{I/S}}$ the thermal equilibrium magnetization of spins I and S, respectively. Both functions are plotted in Fig. 2 for values of $\tau_{\mathrm{D,S}}$ of 65 and 85 ms and a value of $\tau_{\mathrm{D,I}}$ of 10 min. The values for spin S approximately correspond to a sample with 80 or 60% water content, respectively. Conditions in vivo, i.e., the water content of tissue, can be expected to lie between these limits. The value of $\tau_{\mathrm{D,I}}$ for spin I corresponds to a 10 mM solution of a given metabolite in water, again to conditions in vivo. Both functions are nearly independent of $\tau_{\mathrm{D,I}}$ for a concentration range relevant in vivo (1 mM–1 M). The graphs show that the observable signal, even for low metabolite concentrations, is on the same order of magnitude as the diagonal signal in a COSY experiment [10]. Interchanging the indices in Eqs. (1) and (2), the signal for the cross peaks at an f_2-frequency ω_S (water) is obtained. Due to low metabolite concentrations these

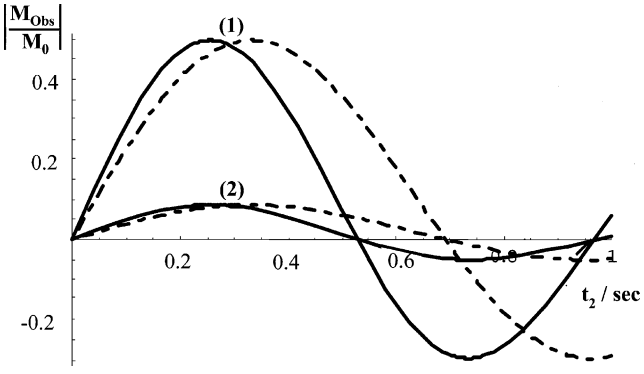

Fig. 2. Development of the signal intensities of the cross peaks in a HOMOGENIZED spectrum for a system of two inequivalent spins I and S. (1) Indicates the signal for p-type coherences according to Eq. (1), and (2) the signal for n-type coherences according to Eq. (2). Solid lines for $\tau_{\mathrm{D,S}} = 65$ ms; dashed lines for $\tau_{\mathrm{D,S}} = 85$ ms; $\tau_{\mathrm{D,I}} = 600$ s for both. M_{obs}/M_0 corresponds to the signal ratio $S_{\mathrm{HOMOGENIZED}}/S_{\mathrm{COSY}}$.

signals are not be observable in vivo and are therefore not further discussed.

For in vivo experiments relaxation has to be taken into account. In the HOMOGENIZED experiment the magnetization relaxes as zero-quantum coherence during t_1. This means that T_2-relaxation is approximately twice as fast (since two spins contribute) as for single-quantum coherences in a COSY experiment, but T_2^+ relaxation is completely removed since the coherences develop as a function of the frequency difference $\omega_I - \omega_S$. Thus, the first part of the experiment (until the second pulse) is more efficient in a HOMOGENIZED sequence when T_2^* is shorter than $T_2/2$. A practical aspect is that the t_1-period can be chosen to be only a few milliseconds, as long as the compromise in resolution is acceptable. In a COSY experiment a longer t_1 is desired due to low J-coupling constants. For best sensitivity, a short t_1 is required and for best resolution, a long t_1. A compromise has to be found for each sample individually. In homogeneous objects with long T_2^*, HOMOGENIZED does not yield better spectra than conventional 1D techniques. To obtain a resolution on the order of a few Hertz in a HOMOGENIZED spectrum, a t_1 on the order of 100 ms is required. This will result in strong signal losses during t_1 and yield spectra of much worse SNR than a 1D spectrum. In very inhomogeneous objects with line widths of several hundreds of Hertz, such as plant leafs or the lung, resolution can be significantly enhanced with the HOMOGENIZED sequence at high magnetic fields.

After the 45°-pulse the observable magnetization increases over a period of several $\tau_{D,S}$. During this time, the build-up competes with T_2^* relaxation. To minimize signal losses a 180°-pulse is inserted and the FID is acquired after an echo time 2Δ on the order of $\tau_{D,S}$ [4]. In the experiment, the echo time has to be optimized for each sample individually.

The HOMOGENIZED signal is dependent on the magnetic field strength since T_2^+ and also T_2 times decrease with the field strength, resulting in stronger losses at higher fields. On the other hand, higher fields allow for shorter t_1 for a given spectral resolution and $\tau_{D,S}$ also decreases with the field. This will roughly compensate shorter relaxation times and make HOMOGENIZED applicable also at more common field strengths. However, the signal gain due to increased M_0 remains, as in all NMR experiments.

Equations (1) and (2) take only dipolar coupling into account. If the contributing spins are J-coupled this will also influence the signal. Ahn et al. [13] have discussed this issue in detail. In the spectra, additional cross peaks due to J-coupling will be observed with the same pattern as in a COSY spectrum, but at different absolute frequencies.

Besides the cross peaks at $\omega_I - \omega_S$ and $\omega_S - \omega_I$ signals will be detected at zero frequency along f_1. This comprises, besides signal from zero-quantum coherences, signal from single-quantum coherences that remains due to imperfect pulses or T_1 relaxation during t_1. Although the HOMOGENIZED sequence performs an intrinsic water suppression (the gradient dephases all single-quantum coherences) the remaining water signal may far exceed the metabolite signals if their concentration is low. In in vivo experiments this may lead to significant contamination (t_1-noise) in the spectra.

Summarizing these properties of HOMOGENIZED spectra, increased resolution can be expected for very inhomogeneous objects without sacrificing significantly the SNR compared to conventional spectroscopic techniques. Summing the f_2 "slices" in the region of interest in the 2D spectrum results in a 1D spectrum with enhanced resolution [4]. In objects with short T_2 times resolution may be limited due to the requirement to choose short t_1 times. If the object is also very inhomogeneous enhanced resolution may be obtained along f_2 due to the local nature of the iZQC signal [9].

3. Results

We have performed HOMOGENIZED experiments with the pulse sequence depicted in Fig. 1 of several phantoms that simulated particular conditions present in vivo, a grape, and the head of a rat.

First, HOMOGENIZED spectra were recorded on a 100 mM solution of γ-aminobutyric acid (GABA) in water (Fig. 3a). At first glance the spectrum looks identical to a COSY spectrum. The three iZQC peaks, created by dipolar coupling between water and each of the three CH_2-groups of GABA, correspond to the three peaks observed in the 1D spectrum. Their shift along f_1 is just the frequency difference $\omega_{H_2O} - \omega_{GABA}$, placing them on a diagonal through the water frequency. In contrast to COSY, these peaks are created by dipolar coupling between two spins. Four peaks that result from additional J-coupling show the same pattern as seen in a COSY spectrum. A spectrum with the center frequency ω_0 set next to the water frequency ω_{H_2O} was shifted along f_2 by $\omega_{H_2O} - \omega_0$ (data not shown). This shift allows identification of the observed peaks as iZQC peaks. In the lower half of the spectrum two weak cross peaks from n-type coherences are visible. Contamination from residual COSY signals due to incomplete dephasing by the gradient were removed by phase cycling the first pulse $(x, -x)$. To simulate the first in vivo condition, namely low metabolite concentration, we recorded a spectrum of a 2.5 mM GABA solution in only 12 min (Fig. 3b). Two peaks, from dipolar coupling between water and the GABA C2 and C3 protons (which we will call H2 and H3 for simplicity), were observed with similar intensities and reasonable SNR. The H4 resonance could not be seperated from the fringe of the

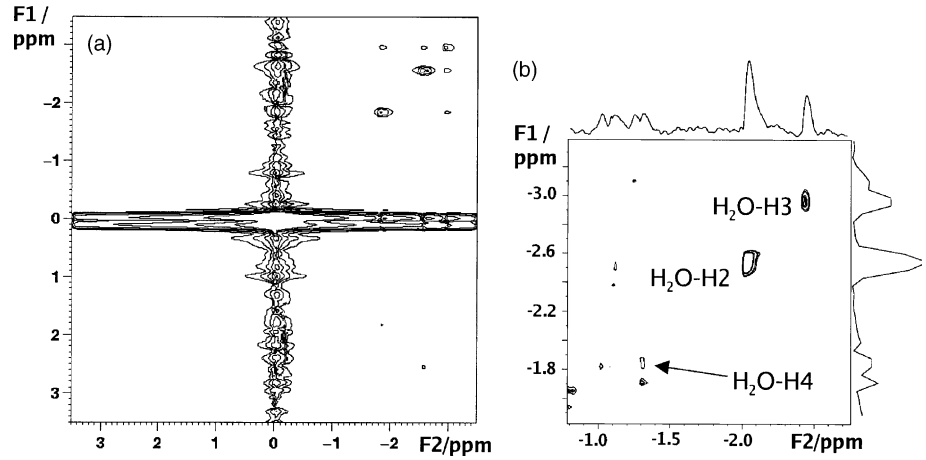

Fig. 3. HOMOGENIZED spectra of GABA solutions in water. (a) For a 100 mM solution 1024 × 128 points were acquired with spectral widths of 7 × 7 ppm in 46 min. Echo time = 220 ms. Center frequency was set to the water resonance. (b) For a 2.5 mM solution 1024 × 64 points were acquired with spectral widths of 7 × 7 ppm in 12 min. Echo time = 220 ms. Center frequency was set at −0.5 ppm from the water line. Pairs of spins that created each respective cross peak by dipolar coupling are labeled. H2, H3, and H4 indicate the corresponding CH_2– groups of GABA. 1D projections of the region of the three signals are shown on top and on the right.

t_1-noise from water. Fig. 3b shows 1D projections of the region with the three resonances. Due to the low number of acquired data points in t_1 and the good shim the resolution is better in the direct dimension in this particular example. However, this spectrum was intended to show that metabolites can be detected at low concentrations. As stated previously HOMOGENIZED does not provide better resolution in homogeneous samples.

To simulate susceptibility gradients present in tissue of living organisms, we used different ''bubble phantoms.'' These consisted of two compartments, separated by a paraffin layer, that each contained a metabolite dissolved in agar gel. One or both compartments also had air bubbles included, which created susceptibility gradients. Fig. 4a shows a sagittal gradient echo image of a bubble phantom containing GABA at 1 M in the lower compartment and sucrose at 1 M with air bubbles in the upper one. The paraffin layer is visible in the center with air bubbles on top. GABA peaks were shimmed to a line width of 0.07 ppm (for the complete multiplet), resulting in a line width of approximately 0.48 ppm for sucrose peaks. Fig. 4b shows a HO-

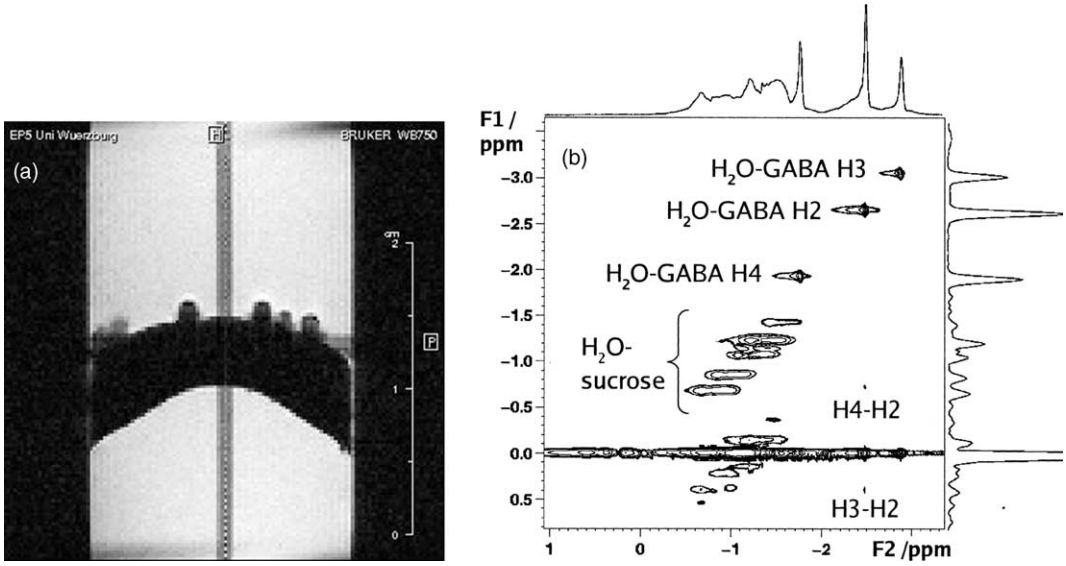

Fig. 4. (a) Sagittal gradient echo image (TE = 1.6 ms, TR = 50 ms, FOV = 30 mm) of the bubble phantom (see text) containing 1 M GABA in the lower compartment and 1 M sucrose in the upper one. Air bubbles can be seen on top of the paraffin layer. The vertical region of signal drop out originated from a coronal slice recorded in the same experiment. (b) HOMOGENIZED spectrum of the bubble phantom with 2048 × 512 points acquired with spectral widths of 8 × 8 ppm in 6 h. Echo time = 100 ms. Center frequency was set −0.4 ppm from the water resonance. Labeling as in Fig. 3b. 1D projections of the region containing the signals are shown on top and on the right.

MOGENIZED spectrum of this phantom. Three cross peaks from the coupling between water and GABA and six from coupling between water and sucrose were detected. The GABA diagonal was shifted with respect to the sucrose diagonal along f_2 on the order of 0.1 ppm. This resulted from very high current in the z-shim-coil necessary to optimize the shim of the GABA resonances. Along the f_2 direction the strongly increased line width for sucrose peaks was obvious. In contrast, along f_1 the peaks of both metabolites had line widths of less than 0.07 ppm, demonstrating the insensitivity to susceptibility gradients of the HOMOGENIZED pulse sequence. Besides the cross peaks between water and metabolites, peaks due to dipolar coupling between different metabolite protons were observed. In Fig. 3b the H4–H2 and the H3–H2 peaks of GABA are labeled. The other four intra-GABA peaks at the f_2-frequencies of H3 and H4 were observed in lower plot layers in the spectrum. At lower concentrations these peaks are not detectable.

To further approach in vivo conditions we recorded spectra with two phantoms containing air inclusions in both compartments and sucrose and *N*-acetylaspartate (NAA) at lower concentrations. With a 100 mM phantom, a peak from the methyl group of NAA and seven isolated resonances of sucrose were resolved in 46 minutes. With a 20 mM phantom the NAA peak and two sucrose resonances were detected in only 6 min (data not shown).

The first application in vivo was performed on an intact grape. In only 6 min we were able to record a spectrum that resolved both the $H1_\alpha$ and the $H1_\beta$ peak of glucose (Fig. 5a). As this experiment was optimized to resolve the H1 resonances in the minimum experimental time, the remaining glucose peaks were only partly resolved. Residual COSY signal was observed in the spectrum, because no phase cycling was applied. Another experiment on the grape with $1024t_1$-increments acquired over 6 h allowed, after Fourier transformation to a 2048×2048 matrix, 10 separated resonances of glucose to be distinguished (spectrum not shown). In this spectrum a reduction in the line widths from about 0.12 ppm in f_2 to about 0.04 ppm in f_1 was observed. Fig. 5b shows an expanded region of a spectrum calculated from this dataset after truncation to $256t_1$-increments and fourier transformation to a 2048×512 matrix. Peaks at 3.22/4.63 and 3.54/5.23 ppm were observed resulting from dipolar coupling with water and *J*-coupling between H1/H2 of the α and β anomer of glucose, respectively. Three resonances at 4.38, 2.96, and 2.78 ppm were putatively assigned to an aspartate moiety. Two further resonances that may originate from lipids were detected at 1.2 and 1.5 ppm (not shown in Fig. 5b).

We have repeated this experiment recording a 2048×256 matrix with spectral widths of 5×5 ppm of the completely deshimmed grape. The resulting spectrum had line widths of about 1.4 ppm along f_2 and 0.07 ppm along f_1 (Fig. 6). In the 1D projection on top no signals are resolved. In the 1D projection on the right the resolution enhancement of the HOMOGENIZED sequence is demonstrated. Even under these conditions

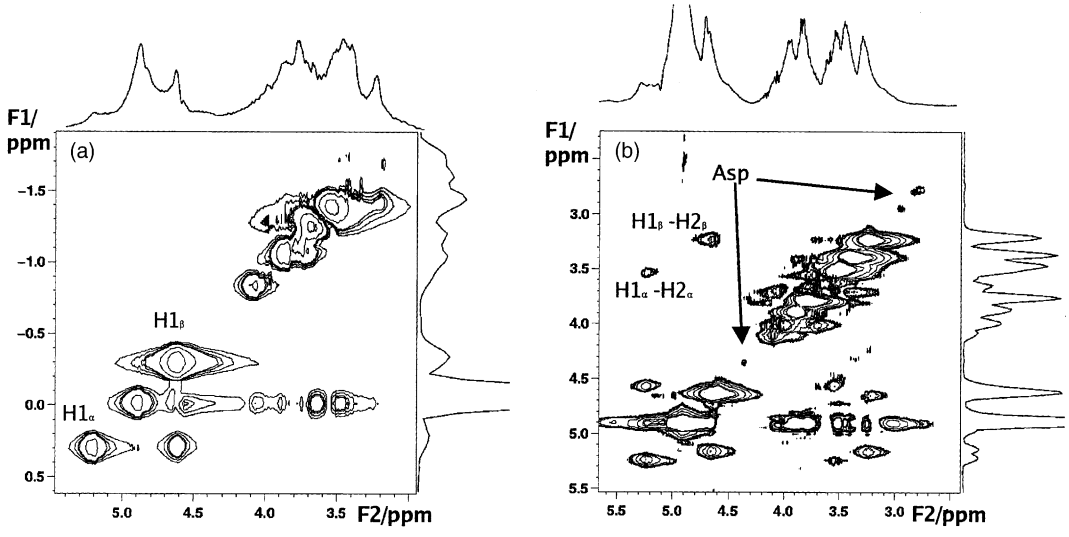

Fig. 5. HOMOGENIZED spectra of a grape. In the plots the water resonance was referenced to 4.9 ppm. 1D projections of the region containing the signals are shown on top and on the right. (a) Expanded region of a spectrum with 2048×64 points acquired with spectral widths of 5×5 ppm in 6 min. Echo time = 260 ms. Center frequency was set 0.3 ppm from the water resonance. $H1_{\alpha/\beta}$ label peaks created by dipolar coupling between water and the respective glucose proton. (b) Zoom of a spectrum with 2048×1024 points acquired with spectral widths of 10×10 ppm in 6 h. Echo time = 100 ms. Center frequency was set −0.4 ppm next to the water resonance. The dataset was truncated to 2048×256 points and zero-filled to 2048×512 points. $H1_{\alpha/\beta}$–$H2_{\alpha/\beta}$ label peaks created by dipolar coupling with water and *J*-coupling between the respective glucose protons. Asp denotes peaks putatively assigned to an aspartate moiety.

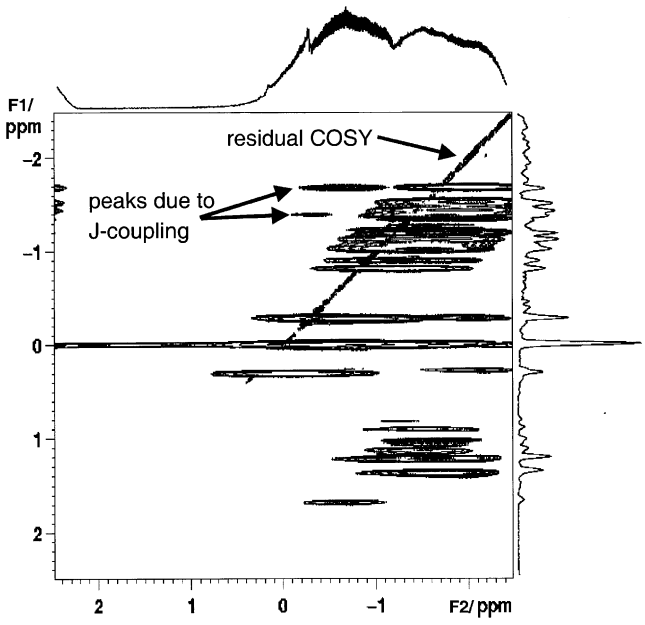

Fig. 6. HOMOGENIZED spectrum of the deshimmed grape with 2048×256 points acquired with spectral widths of 5×5 ppm in 24 min. Echo time = 200 ms. Center frequency was set −0.2 ppm from the water resonance. In the plots the water resonance was referenced to 4.9 ppm. Residual COSY signal was observed because no phase cycle was applied. Additional peaks due to *J*-coupling between H1 and H2 for both anomers of glucose are indicated. 1D projections of the region containing the signals are shown on top and on the right.

the H1 resonances of both glucose anomers were resolved and peaks due to *J*-coupling (H1–H2 for both anomers) were observed in the 2D spectrum.

Finally, we have applied the HOMOGENIZED sequence to record a spectrum of a rat brain in vivo. Fig. 7a shows a sagittal gradient echo image of the rat in the resonator. The brain was the largest organ in the resonator, besides the tongue, the eyes (not visible in Fig. 7a), and muscles. The sensitivity of the coil strongly decreased at the edges of the field of view. This allowed for the rough estimation that the main signal contribution of an unlocalized HOMOGENIZED spectrum came from the brain. Fig. 7b shows a global 1D spectrum of the head. Due to the line shape water suppression was not possible. Metabolite signals were not resolved. With the global HOMOGENIZED sequence we were able to resolve peaks of NAA, choline, and creatine in 12 min (Fig. 7c). In a corresponding spectrum recorded in 1.5 h with 16 averages peaks for glutamate and lipids were detected in addition (spectrum not shown). We have recorded a localized 1D spectrum of a $(7\,\mathrm{mm})^3$ volume (see Fig. 7a) from the central brain for comparison (Fig. 7d). Peaks from NAA, choline, creatine, glutamate, *myo*-inositol, and lipids were detected as indicated in Fig. 7d. The HOMOGENIZED spectrum of a brain phantom containing the major brain metabolites at typical in vivo concentrations showed the same peaks as the spectrum of the rat (Fig. 8a). Due to more complex structures, motion and flow artifacts, and shorter T_2 times in the rat the spectrum of the phantom was of better quality. Already after 12 min, all peaks observed in the rat after longer scan times were detected. Additionally, a weak peak of the methyl group of the low concentration alanine and one peak each of a C_β-proton of aspartate and NAA were observed. Glutamate signals were observed with increased intensities, allowing for identification of one very weak peak originating from *J*-coupling between the C_β- and C_γ-protons.

For comparison we have recorded a conventional COSY spectrum with water presaturation using similar spectral widths and number of t_1 increments as for the HOMOGENIZED spectrum. Fig. 8b shows a plot of this spectrum acquired in 12 min. Diagonal peaks of all metabolites were observed. The main difference from the HOMOGENIZED spectrum is that peaks from *J*-coupled spins were significantly stronger in the COSY spectrum. Weak cross peaks from alanine and glutamate were found in lower plot layers. Besides the slightly better sensitivity in this homogeneous sample, COSY does not yield more information than HOMOGENIZED. As a more complex phantom we have used an identical brain phantom with included air bubbles throughout the gel. Satisfactory water suppression was not possible. Thus, a COSY spectrum could not be acquired. In contrast, the HOMOGENIZED spectrum (Fig. 8c) still resolved all metabolite signals although the quality decreased compared to the homogeneous phantom.

4. Discussion

It has been shown previously using high resolution spectrometers that double-quantum CRAZED spectra can be recorded of 20 mM solutions [9] and that *J*-coupling can be observed [9,13]. Our experiments on GABA dissolved in water show that it is possible to obtain HOMOGENIZED spectra with imaging hardware in a few minutes. Additional cross peaks allow the detection of *J*-coupling between different protons, but coupling constants cannot be determined since multiplets are not resolved. The spectrum of the 2.5 mM GABA solution shows that iZQC spectroscopy is not limited to high concentrations. Metabolites at in vivo concentrations are also accessible with this technique. Vathyam et al. [4] have demonstrated that linear field inhomogeneities over the sample volume do not lead to line broadening in the indirect dimension in HOMOGENIZED spectra recorded with high resolution hardware. Our experiments on the bubble phantoms show that even line broadening due to complex susceptibility gradients in a sample can be almost completely removed

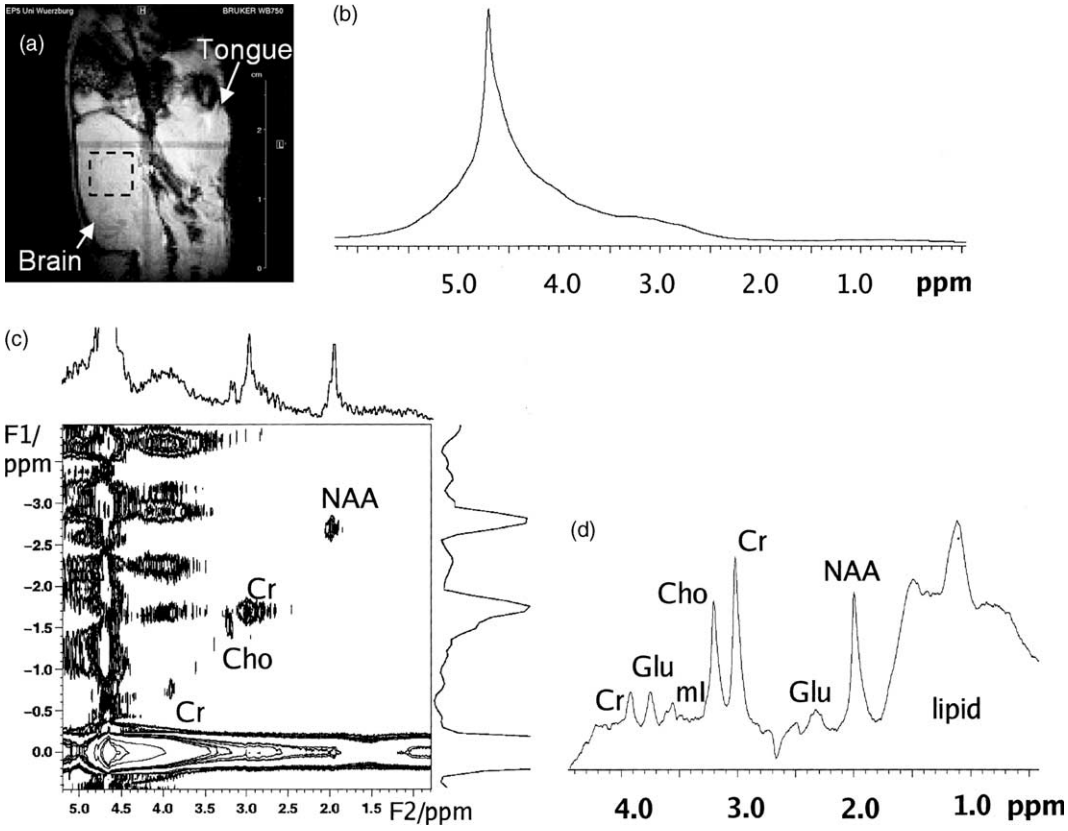

Fig. 7. (a) Sagittal gradient echo image (TE = 2.3 ms, TR = 60 ms, FOV = 40 mm) of the head of a female Fisher rat in vivo. Brain and tongue are indicated; dashed square shows the position of the voxel from which a localized 1D spectrum was recorded. (b) Global 1D spectrum of the head of the rat in vivo. Only the water line is resolved. (c) HOMOGENIZED spectrum of the rat brain in vivo with 2048 × 64 points acquired with spectral widths of 8 × 8 ppm in 12 min. Echo time = 60 ms. Center frequency was set −1.0 ppm from the water resonance. In the plot the water resonance was referenced to 4.7 ppm. Metabolites that created peaks by dipolar coupling with water are labeled. A 1D projection of f_1 slices of the region with the signals is shown on top. A 1D projection of f_2 slices of the region between the choline and the NAA signals is shown on the right. (d) Localized PRESS spectrum from a $(7\,\text{mm})^3$ volume indicated in (a). The water signal has been arbitrarily referenced to 4.7 ppm. Peaks from lipids, NAA, glutamate (Glu), creatine (Cr), choline (Cho), and *myo*-inositol (mI) were observed.

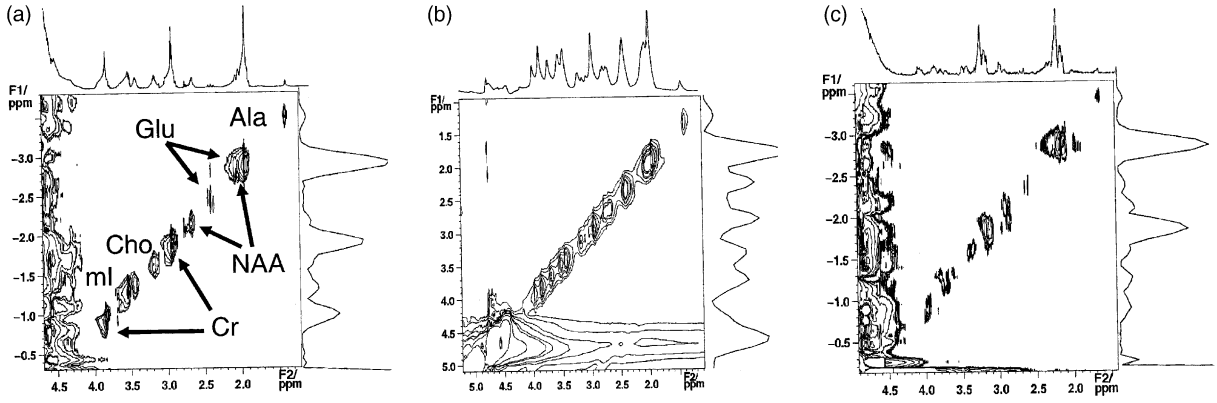

Fig. 8. (a) HOMOGENIZED spectrum of the brain phantom (agar gel without air bubbles). Acquisition parameters were chosen identical to the spectrum of the rat brain (Fig. 7c). (b) COSY spectrum (with water presaturation) of the brain phantom. (c) HOMOGENIZED spectrum of the brain phantom with air bubbles. Acquisition parameters as in (a).

(Fig. 4). It is not possible to approach the natural line width, as in [4], since the inhomogeneities are only refocused over a scale larger than a typical correlation distance [9], which is on the order of 150 μm in our experiments. Thus, averaged over the sample, line widths of 0.07 ppm remain.

Recent simulations on the effects of the orientation of field inhomogeneities on line widths in CRAZED spectra [14], again for high resolution conditions, have shown that line broadening due to inhomogeneities perpendicular to the main field are reduced to 20 Hz in iZQC CRAZED spectra, but to 6 Hz for inhomogeneities parallel to the field. iZQC cross peaks can be even completely destroyed if the resulting modulation of the field (inhomogeneity plus correlation gradient) lies along the magic angle. For air–gel interfaces, present in the bubble phantoms, internal field gradients on the order of several hundreds of millitesla per meter have to be taken into account. This is on the same order of magnitude as the applied correlation gradient. However, the spherical shape of the bubbles and their roughly random distribution along the paraffin layer lead us to the assumption that the net effect of the internal gradients can be neglected. However, the increased line widths for perpendicular inhomogeneities in the simulations do not affect our spectra, as line widths under in vivo imaging conditions are larger than 20 Hz.

Summarizing the bubble phantom experiments, we have shown that line widths in HOMOGENIZED spectra from difficult to shim samples can be reduced along the indirect dimension and thus allow resolution of individual resonances of metabolites. The bubble phantoms mimic tissue present in the lung or in leaves of plants. The detection of peaks from metabolites at a concentration of only 20 mM promises that NMR spectroscopy of these tissues may become possible with this new strategy. However, air inclusions in the phantoms were on the order of 1 mm. In tissue, the structures causing susceptibility differences may be as small as 10–100 μm. Decreasing the correlation distance (by increasing the gradient) will allow compensation for structures below 50 μm. Practical applicability has to be tested for each target tissue. The general feasibility for in vivo applications is shown by our experiments with the grape and the rat.

Our spectra of the grape are to our knowledge the first in vivo applications of iZQC spectroscopy. They show that it is possible in 6 min to resolve peaks only 0.3 ppm distant from the water line. The spectrum with the higher resolution along f_1 (Fig. 5b) suggests the potential to resolve peaks closer to the water line and emphasizes the fundamental property of iZQC spectra of enhancing resolution along the indirect dimension. Acquisition of comparable resolutions with conventional 2D sequences, such as COSY or SECSY, would be extremely difficult, if not impossible. In any case, excellent water suppression would be crucial, which is challenging under imaging conditions. The particular value of iZQC spectra for in vivo application is clearly demonstrated by the spectrum of the deshimmed grape. Long shimming procedures that are essential for conventional spectroscopy can be significantly shortened. For experiments on animals additional scan time can be gained.

The HOMOGENIZED spectra of the rat brain are to our knowledge the first iZQC spectra of a living animal. Peaks of five major metabolites were detected that are abundant at millimolar concentrations in the brain [15]. Lipid signal is only detected after long scan times, although extracranial lipids are abundant at higher concentration than the observed metabolites. This can be explained by two reasons. First, lipids have shorter T_2 relaxation times than metabolites. Thus, their signal is strongly attenuated after an echo time of 60 ms. Second, lipids are not dissolved in high concentrations of water as other metabolites. The concentration of water, creating the iZQC signal, is lower than in the brain. Consequently, less signal is produced.

Comparison of the in vivo spectrum with the spectrum of the brain phantom shows that all metabolites with expected proton concentrations of more than 5 mM are observed. The signal intensities correspond to the expected concentrations in both the phantom and the brain. Absolute quantification, however, is difficult. The observed signal is a function of the concentration, the relaxation time, and the interaction with water spins. If the distribution of the metabolites is homogeneous, the interaction with water is the same for all metabolites. Thus, if the relaxation times are known the concentration can be estimated. If one metabolite signal is used as a reference, relative concentrations can be determined. HOMOGENIZED is a powerful tool to detect metabolites that accumulate at higher concentration, such as lactate produced under oxygen deprivation or proline and trehalose produced in plants under osmotic stress.

The brain spectrum demonstrates again that spectra can be obtained without time-consuming setup procedures. However, the limit of this straight forward application of HOMOGENIZED to living objects is also shown. With the localized 1D spectrum, more information can be gained in shorter time, demonstrating that for well-shimmed objects conventional spectroscopy is superior to iZQC methods. Our experiments with the rat and the brain phantoms show that in homogeneous objects, such as the phantom without air bubbles, COSY yields spectra of better quality and provides additional information in terms of resolved scalar couplings. In inhomogeneous objects, however, COSY is not applicable but HOMOGENIZED resolves signals from metabolites. Comparing the HOMOGENIZED spectrum of the brain with the global 1D spectrum, the advantages of iZQC methods become obvious. Global water suppression is not possible due to the inhomogeneity of the head. Thus, no metabolite peaks are observed in the global 1D spectrum (Fig. 7b). In the global HOMOGENIZED spectrum the resolution is enhanced and metabolite signals are resolved (Fig. 7c), yielding new information. In this particular

example the voxel in the brain is separated several millimeters from air containing structures allowing for a local shim and water suppression. Here, conventional localized spectra yield better results than iZQC methods. However, conventional spectroscopy depends crucially on the shim. High field applications are limited to large homogeneous structures, such as the brain or muscles. As soon as structures become too small for a local shim the applicability of conventional spectroscopy breaks down. Here lies the potential of future iZQC applications. However, to compare the method to conventional spectroscopy further developments are necessary.

iZQC spectroscopy has the potential to be further improved. So far we have only optimized gradient strength and echo time and phase cycled only the first pulse. Better spectra may be gained with improved pulse sequences. These may comprise additional phase cycles on the second and third pulse that have been shown to significantly improve iZQC spectra [12,14]. Further options are the use of composite pulses or spoiler gradients or the combination of HOMOGENIZED with an additional water suppression module before the acquisition time. To exploit the full potential of iZQC spectroscopy a localized version of HOMOGENIZED will be required. This may open the possibility of applying iZQC spectroscopy to other organs.

5. Conclusions

Summarizing our results, we conclude that the application of HOMOGENIZED in vivo is possible. Line broadening due to susceptibility gradients can be essentially eliminated. Resolution in spectra of objects that cannot be shimmed, as in our bubble phantoms, is significantly enhanced along the indirectly detected dimension. Metabolites at millimolar concentrations can be detected in vivo. Time-consuming setup procedures can be shortened, since iZQC spectra are insensitive to the shim. The development of localized versions of HOMOGENIZED will make applications to other organs possible. NMR spectroscopy of air containing tissues, such as the lungs of mammals or leaves of plants, may become feasible with this strategy.

6. Experimental

All experiments were performed on a Bruker AVANCE 750WB spectrometer with a 89 mm vertical bore operating at a field strength of 17.6 T. Spectra were recorded with Bruker gradient systems and probeheads comprising bird cage resonators with an inner diameter of 15 mm for the GABA solutions, 20 mm for the bubble phantoms and the grape, and 38 mm for the rat and the brain phantoms. The HOMOGENIZED sequence [4] was used as shown in Fig. 1. The correlation gradient was switched on for 1 ms with a strength of 100 mT/m, except for the 100 mM GABA sample, the brain phantoms and the rat, where a value of 60 mT/m was used. Spectral widths, number of acquired points and echo time were chosen individually for each sample. A repetition delay of 5 s was chosen throughout, except for the spectrum of the grape with 1024 t_1-increments, where a delay of 10 s was used. A phase cycle of the first pulse $(x, -x)$ was applied in experiments with more than one scan per t_1-increment to suppress residual COSY peaks. Processing was preformed with XWINNMR (Bruker, Rheinstetten, Germany). Raw data were zero filled by a factor of two. The spectrum of the grape with 1024 t_1-increments was truncated to 256 t_1-increments and zero-filled to 512 increments. For the 2.5 mM GABA spectrum, the truncated spectrum of the grape, and the spectra of the brain phantoms an additional baseline correction was applied [16]. 1D projections of the spectra were calculated by summing the respective slices of the 2D spectrum over a region of interest. This region of interest has to be chosen for each spectrum individually and comprises the region with the relevant cross peaks. Summing over the whole spectrum may render the projections useless since, along f_1, t_1-noise from water and, along f_2, non-zero-quantum signal at zero frequency will be included.

For the COSY spectrum 2048×64 data points were acquired with spectral widths of 10×10 ppm. Gradient coherence selection around the second pulse and presaturation of the water frequency for 200 ms were applied. The repetition delay was 2.5 s. Four scans were accumulated per t_1-increment.

The localized 1D spectrum was recorded with a PRESS sequence [17] (TE = 50 ms). One hundred and twenty-eight scans were accumulated in 2 min. A FASTMAP [18] shim was performed for an $(8\,\text{mm})^3$ volume in the central brain, water suppression was performed with a CHESS module [19].

A female Fisher rat was anesthetized with 2% isoflurane and kept in the Bruker animal handling system for the spectra of the brain.

For bubble and brain phantoms metabolites were dissolved in agar gel and placed in 20 mm NMR tubes. The brain phantoms contained eight metabolites at their expected in vivo concentrations [15]: 10 mM NAA, 2.5 mM choline, 10 mM creatine, 15 mM glutamate, 8 mM inositol, 1.4 mM alanine, 2 mM GABA, and 1.4 mM aspartate.

Acknowledgments

The 17.6 T wide bore spectrometer was funded by the Deutsche Forschungsgemeinschaft under Grant HA 1232/13-1. The authors would like to thank

Dr. Kristian Schweimer for providing a baseline correction routine.

References

[1] See for example: R. de Graaf, In Vivo NMR Spectroscopy, Wiley, Chichester, 1998.
[2] C.A. Meriles, D. Sakellariou, H. Heise, A.J. Moule, A. Pines, Approach to high-resolution ex situ NMR spectroscopy, Science 293 (2001) 82–85.
[3] M. Munowitz, A. Pines, Multiple-quantum nuclear magnetic resonance spectroscopy, Science 233 (1986) 525–531.
[4] S. Vathyam, S. Lee, W.S. Warren, Homogeneous NMR spectra in inhomogeneous fields, Science 272 (1996) 92–96.
[5] Y.-Y. Lin, S. Ahn, N. Murali, W. Brey, C.R. Bowers, W.S. Warren, High-resolution, >1 GHz NMR in unstable magnetic fields, Phys. Rev. Lett. 85 (2000) 3732–3735.
[6] G. Deville, M. Bernier, J.M. Delrieux, NMR multiple echoes observed in solid ^{3}He, Phys. Rev. B 19 (1979) 5666–5688.
[7] J. Jeener, A. Vlassenbroek, P. Broekaert, Unified derivation of the dipolar field and relaxation terms in the Bloch-Redfield equations of liquid NMR, J. Chem. Phys. 103 (1995) 1309–1332.
[8] M.H. Levitt, Demagnetization field effects in two-dimensional solution NMR, Concepts Magn. Reson. 8 (1996) 77–103.
[9] W.S. Warren, W. Richter, A.H. Andreotti, S. Farmer, Generation of impossible cross-peaks between bulk water and biomolecules in solution NMR, Science 262 (1993) 2005–2009.
[10] S. Lee, W. Richter, S. Vathyam, W.S. Warren, Quantum treatment of the effects of dipole–dipole interactions in liquid nuclear magnetic resonance, J. Chem. Phys. 105 (1996) 874.
[11] W. Richter, W.S. Warren, Intermolecular multiple quantum coherences in liquids, Concepts Magn. Reson. 12 (2000) 396–409.
[12] S. Ahn, N. Lisitza, W.S. Warren, Intermolecular zero-quantum coherences of multi-component spin systems in solution NMR, J. Magn. Reson. 133 (1998) 266–272.
[13] S. Ahn, W.S. Warren, S. Lee, Quantum treatment of intermolecular multiple-quantum coherences with intramolecular *J* coupling in solution NMR, J. Magn. Reson. 128 (1997) 114–129.
[14] S. Garrett-Roe, W.S. Warren, Numerical studies of multiple quantum coherences: high-resolution NMR in inhomogeneous fields and contrast enhancement in MRI, J. Magn. Reson. 146 (2000) 1–13.
[15] V. Govindaraju, K. Young, A.A. Maudsley, Proton NMR chemical shifts and coupling constants for brain metabolites, NMR Biomed. 13 (2000) 129–153.
[16] M.A. Friedrichs, A model-free algorithm for the removal of baseline artifacts, J. Biomol. NMR 5 (1995) 147–153.
[17] P.A. Bottomley, Spatial localization in NMR spectroscopy in vivo, Ann. N. Y. Acad. Sci. 508 (1987) 333–348.
[18] R. Gruetter, Automatic localized in vivo adjustment of all first- and second-order shim coils, Magn. Res. Med. 29 (1993) 804–811.
[19] A. Haase, J. Frahm, W. Hanicke, D. Matthaei, ^{1}H NMR chemical shift selective (CHESS) imaging, Phys. Med. Biol. 30 (1985) 341–344.